Project No. 037005

CECILIA

Central and Eastern Europe Climate Change Impact and Vulnerability Assessment

Specific targeted research project

1.1.6.3.I.3.2: Climate change impacts in central-eastern Europe

D4.3: Analyses of the CECILIA driving-model simulations, links between large-scale circulation patterns and extreme events

Due date of deliverable: 1st June 2008
Actual submission date: 18th November 2008

Start date of project: 1st June 2006   Duration: 36 months

Lead contractor for this deliverable: Swiss Federal Institute of Technology (ETHZ)

Revision [final]

CECILIA Deliverable 4.3: Analyses of the CECILIA driving-model simulations, links between large-scale circulation patterns and extreme events

Lead partner for deliverable: ETHZ

Contributing partners: DMI, NMA, AUTH

Final revision November 18, 2008

D4.3.0 Overview

The present report contains sub-reports from the individual institutions (ETHZ, DMI, NMA, AUTH) contributing to deliverable D4.3 of CECILIA WP4.

The deliverable focused on the analysis of the CECILIA driving-model simulations and was performed in coordination with D4.2. The aim was to assess the quality of the CECILIA driving-model simulations with regard to features relevant for extreme events in comparison with pre-existing RCM data (PRUDENCE, ENSEMBLES) and with observational data sets (ECA&D; Klein Tank et al. 2002; http://eca.knmi.nl/). Moreover, links between large-scale circulation patterns and extreme events were investigated.

In addition to the observational data sets defined in D4.1 (ECA&D, local observations from the individual partners), the gridded observations from ENSEMBLES WP5.1 (Haylock et al. 2008) have been included in the indices analyses of WP4.

D4.3.1 ETHZ and DMI

In tight collaboration, DMI and ETH were calculating the extreme indices for the CECILIA driving models from CNRM (ARPEGE) and ICTP (RegCM). This included again a thorough crosschecking of the Matlab and R scripts to ensure the consistent calculation of the indices from the different data sets. At the time of the preparation of the deliverable, the transient run from ICTP was not yet available for the analysis. Thus we concentrate here on the RegCM ERA-40 run and the transient ARPEGE run, while the analysis of the RegCM transient run will follow later.

Moreover, the indices from the newly included gridded observations from ENSEMLES have been computed and are included in the analysis. This data extends the observational data sets defined in D4.1. It is based on the ECA&D station data, but includes more stations than are freely available on the ECA&D database.

The following two subsections present results from the validation and the model inter-comparison separately for selected temperature and precipitation indices.

D4.3.1.1 Temperature indices
Figure 1 displays Taylor plots (Taylor 2001) showing the spatial standard deviations σ (normalized by the standard deviation of the observations) and the correlation coefficients r of the PRUDENCE and ENSEMBLES RCMs, as well as the CECILIA driving models compared against the ENSEMBLES gridded observations. The statistics are derived from the annual indices values of the period 1961–1990 and for the East European domain (16°E–30°E, 44°N–55°N). Note that the CECILIA driving run from ICTP (i.e., the ERA-40 run) coincides with the respective ENSEMBLES run.

Generally, the spatial agreement between the models and the observations is very good for mean, maximum and minimum temperature (both in terms of the spatial variability and the spatial correlation). It is also noteworthy that the CECILIA models are very close to the observations in terms of spatial variability. The spread between the models is larger for the daily temperature range, with most models showing larger spatial variability compared to the observations. Moreover, the spatial correlation between the gridded observations and the models is also slightly lower (0.6–0.85).
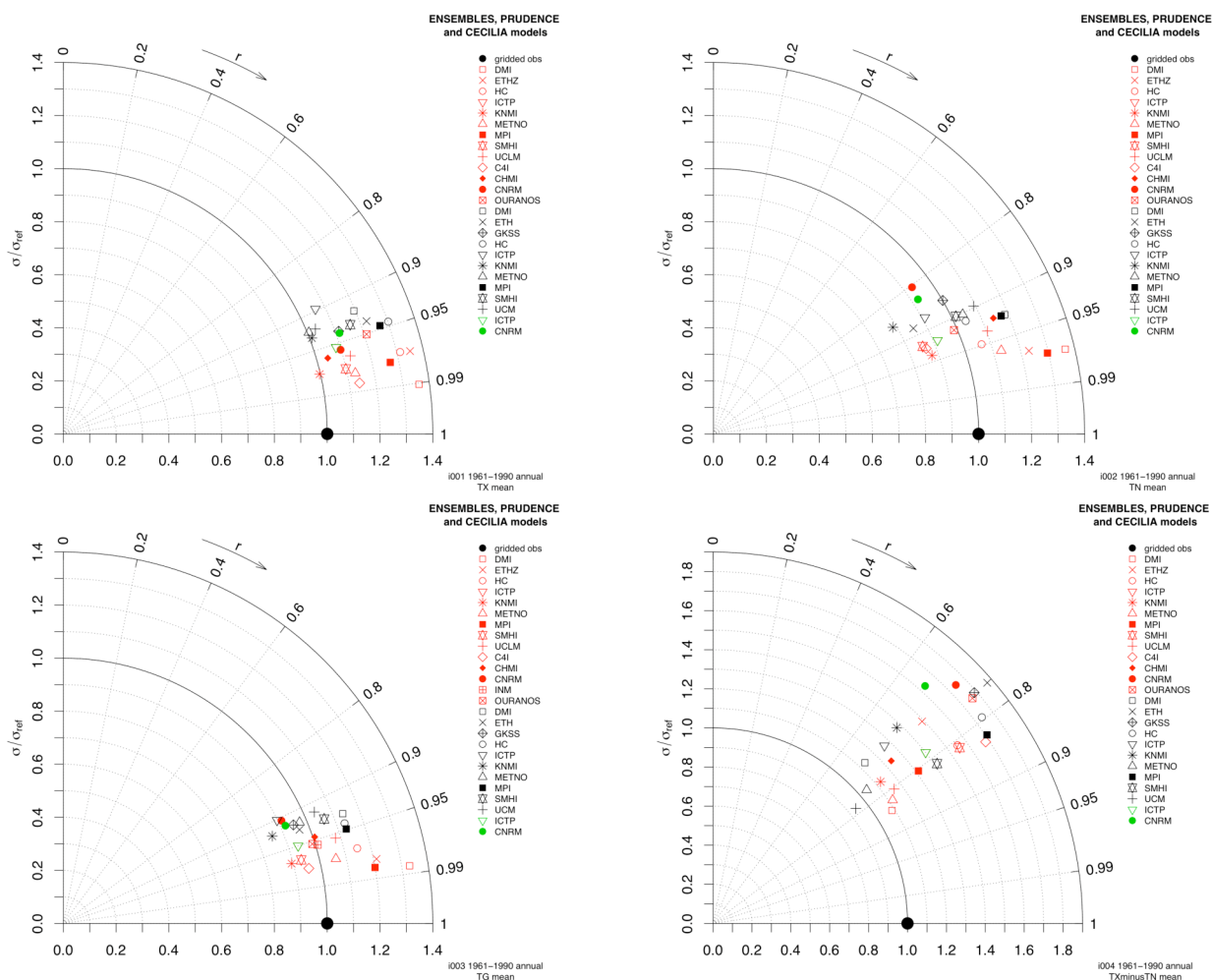

Figure 1. *Taylor plots of the ENSEMBLES (red symbols) and PRUDENCE (black symbols) RCMs, as well as the CECILIA driving runs (green symbols) compared against the ENSEMBLES gridded observations. (Top left) maximum temperature, (top right) minimum temperature, (bottom left) mean temperature, (bottom right) daily temperature range. Displayed are annual values for the period 1961–1990 and for the East European domain (16°E–30°E, 44°N–55°N). σ denotes the spatial standard deviations (normalized by the standard deviation of the observations) and r the correlation coefficients.*

Figure 2 shows a comparison of different heat and cold wave indices (i.e., mean heat wave occurrence, 90th percentile-based maximum heat wave duration, mean cold wave occurrence, 10th percentile-based maximum cold wave duration) from the ECA&D station data, the ENSEMBLES gridded observations, and the CECILIA driving models. Moreover, Figure 3 shows the respective spatial Taylor plots for these indices from the PRUDENCE and ENSEMBLES RCMs, as well as the CECILIA driving models compared against the ENSEMBLES gridded observations. The models perform relatively well for the mean heat and cold wave occurrence, although the spread between the models is large (Figure 3). The results are worse for the percentile-based heat and cold wave durations. In these cases, the spatial correlations between the models and the gridded observations decrease to around zero, with some models even showing negative correlations. However, one has to note that the spatial pattern in the gridded

observations is quite noisy for these percentile-based indices, which might be difficult to be reproduced by the models (Figure 2). On the other hand, the mean heat and cold wave occurrences show a west–east gradient, which is also relatively well captured by the models.
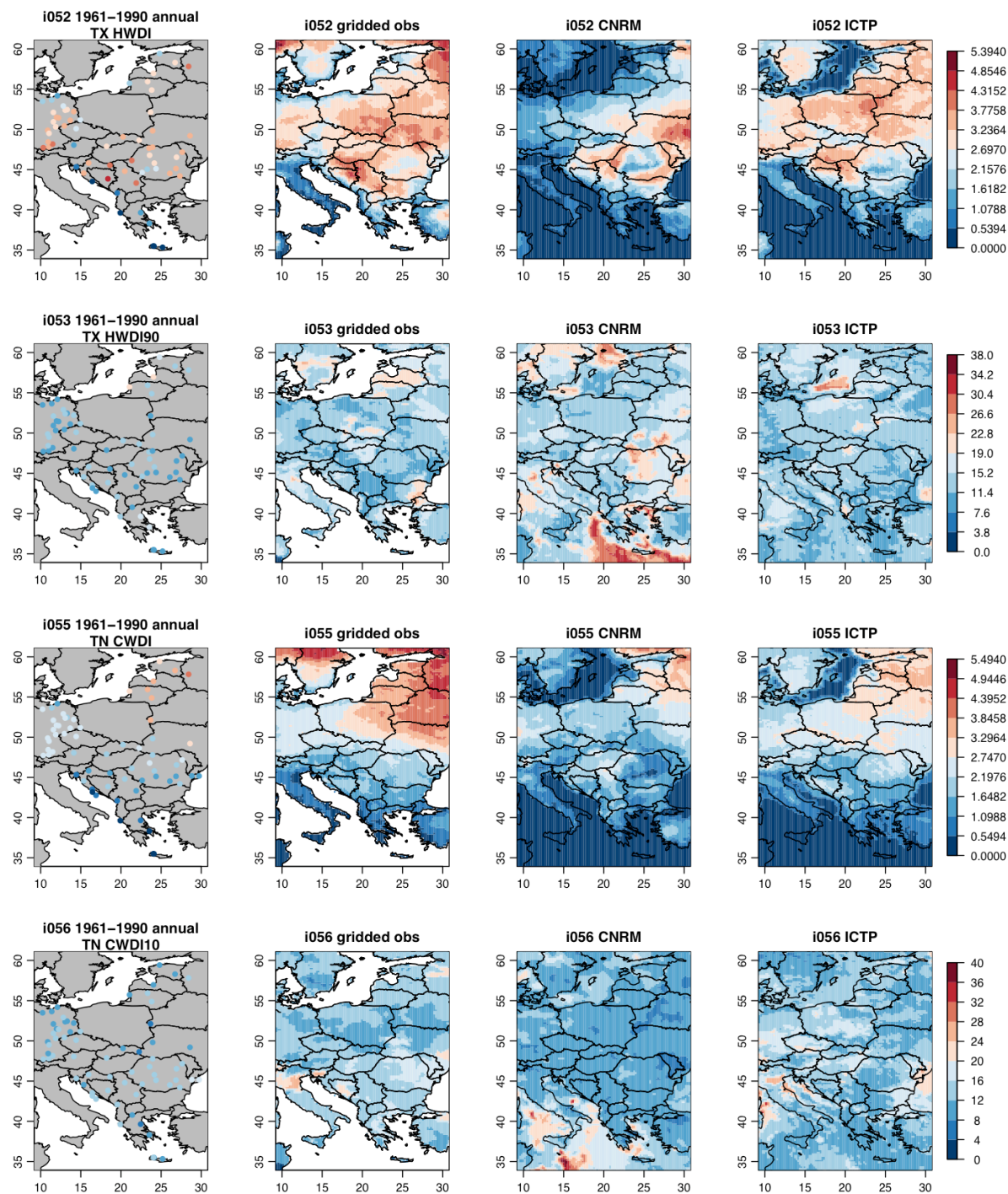

Figure 2. *Comparison of different heat and cold wave indices from the ECA&D station data, the ENSEMBLES gridded observations, and the CECILIA driving models from CNRM and ICTP. (1st row) mean heat wave occurrence [%], (2nd row) 90th percentile-based maximum heat wave duration [days], (3rd row) mean cold wave occurrence [%], (4th row) 10th percentile-based maximum cold wave duration [days].*
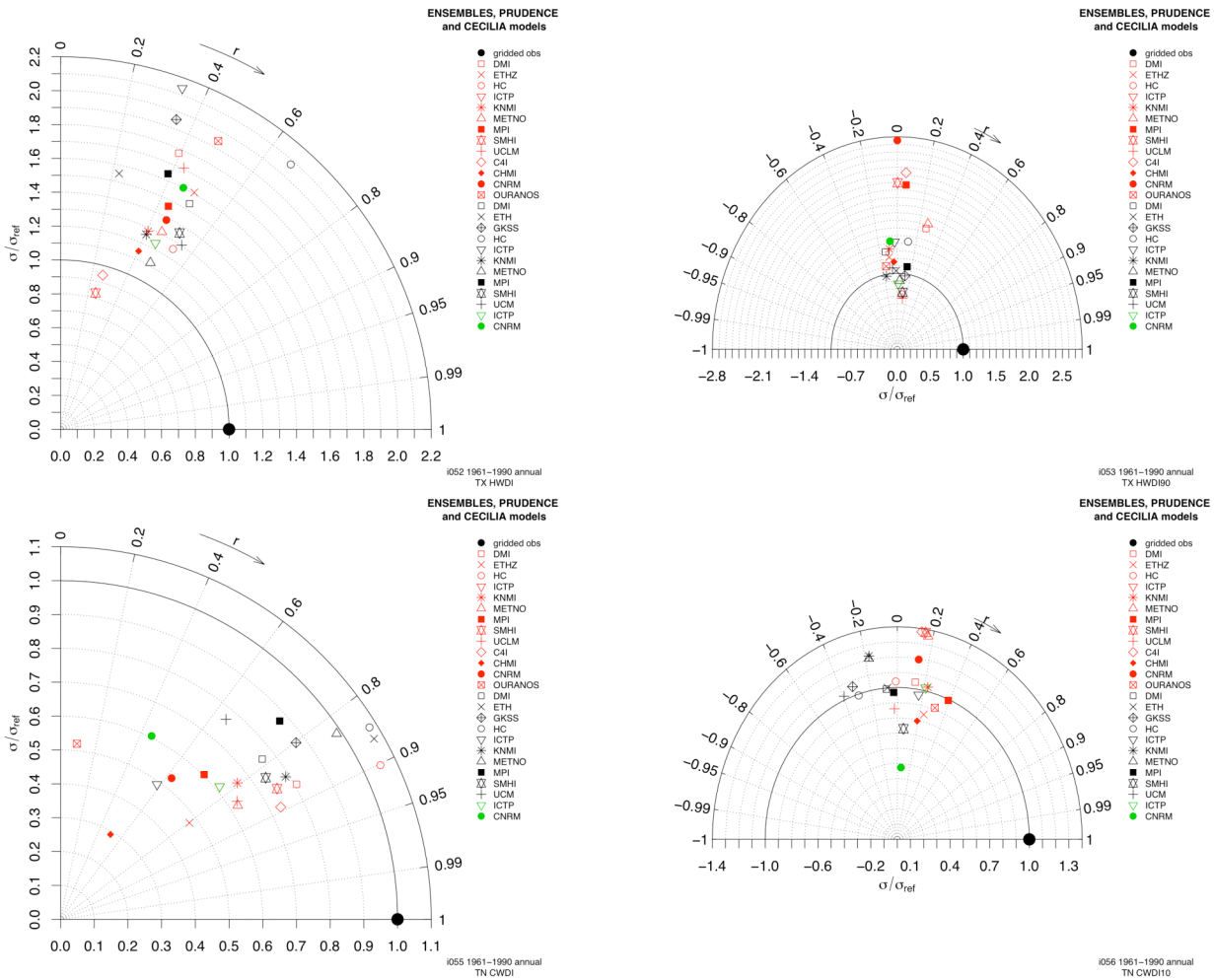
Figure 3. *As Figure 1, but for the different heat and cold wave indices displayed in Figure 2. (Top left) mean heat wave occurrence, (top right) 90th percentile-based maximum heat wave duration, (bottom left) mean cold wave occurrence, (bottom right) 10th percentile-based maximum cold wave duration.*

Figure 4 shows a selection of further temperature indices as defined in D4.1 (i.e., growing degree days, percentage of frost days, percentage of summer days). For all these indices, the CECILIA driving simulations perform well and show similar spatial patterns and absolute values as the gridded observations.
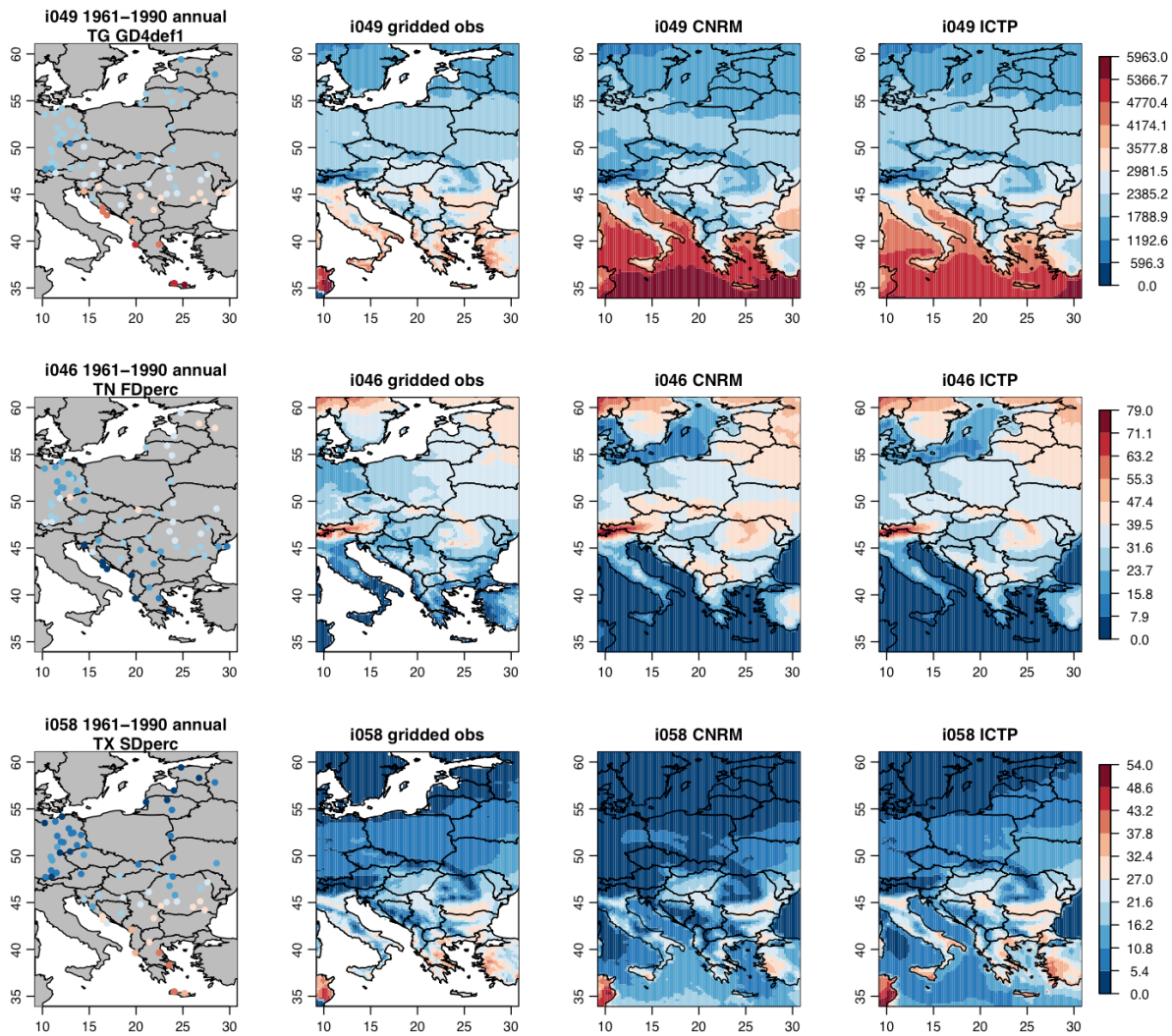
Figure 4. *Comparison of other temperature indices from the ECA&D station data, the ENSEMBLES gridded observations, and the CECILIA driving models. (Top row) growing degree days [°C], (middle row) percentage of frost days [%], (bottom row) percentage of summer days [%].*

D4.3.1.2 Precipitation indices

Similarly as for the temperature indices above, this subsection presents some preliminary results for a selection of precipitation indices.

Figure 5 shows the spatial Taylor plots of mean precipitation and mean wet-day precipitation from the PRUDENCE and ENSEMBLES RCMs, as well as the CECILIA driving models compared against the ENSEMBLES gridded observations. The spread between the models is relatively large with a tendency of the models to have larger spatial variability compared to the gridded observations. However, the CECILIA driving models (green symbols) perform reasonably well compared to the other model datasets.
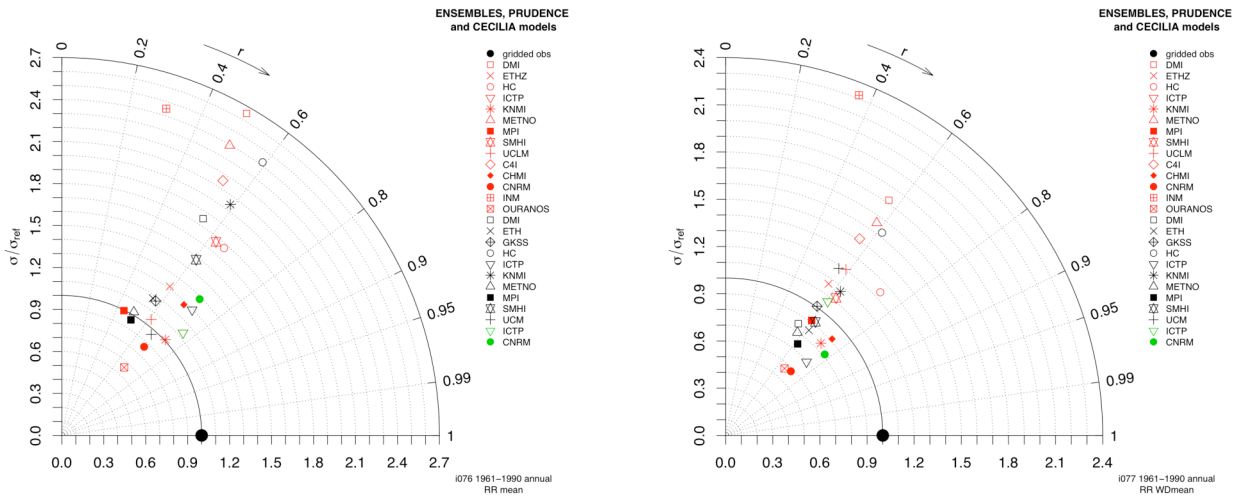
Figure 5. *As Figure 1, but for (left) mean precipitation, and (right) mean wet-day precipitation.*

Figure 6 displays a selection of derived precipitation indices (i.e., max. number of consecutive dry days, max. number of consecutive wet days, median dry spell length, median wet spell length), and Figure 7 the respective Taylor plots for these indices. The CECILIA models perform quite well in case of max. number of consecutive dry days and median dry spell length. Both models show a slight negative bias for the max. number of consecutive dry days in the northern parts of the region (Figure 6). CNRM shows (see Figure 7) too high (low) spatial variability for the max. number of consecutive wet days (median wet spell length), in connection with a positive bias for both indices.

Some further precipitation indices are shown in Figure 8 (i.e., greatest 1-day total rainfall and percentage of wet days > 5mm). The agreement between the CECILIA models and the observations is good for the percentage of wet days > 5mm. Both models show a negative bias for the greatest 1-day total rainfall.
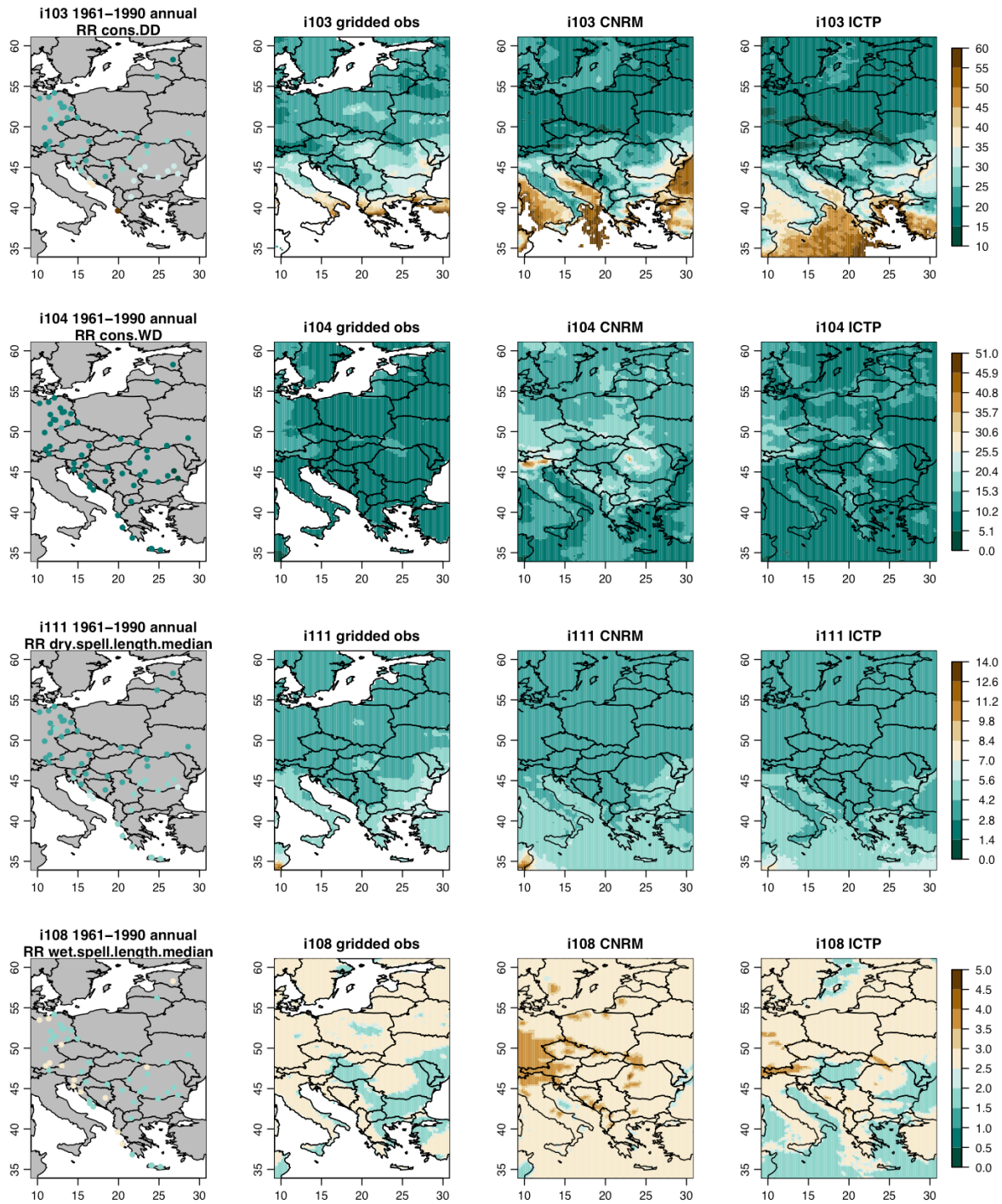
Figure 6. *Comparison of different derived precipitation indices from the ECA&D station data, the ENSEMBLES gridded observations, and the CECILIA driving models from CNRM and ICTP. (1st row) Max. number of consecutive dry days [days], (2nd row) max. number of consecutive wet days [days], (3rd row) median dry spell length [days], (4th row) median wet spell length [days].*
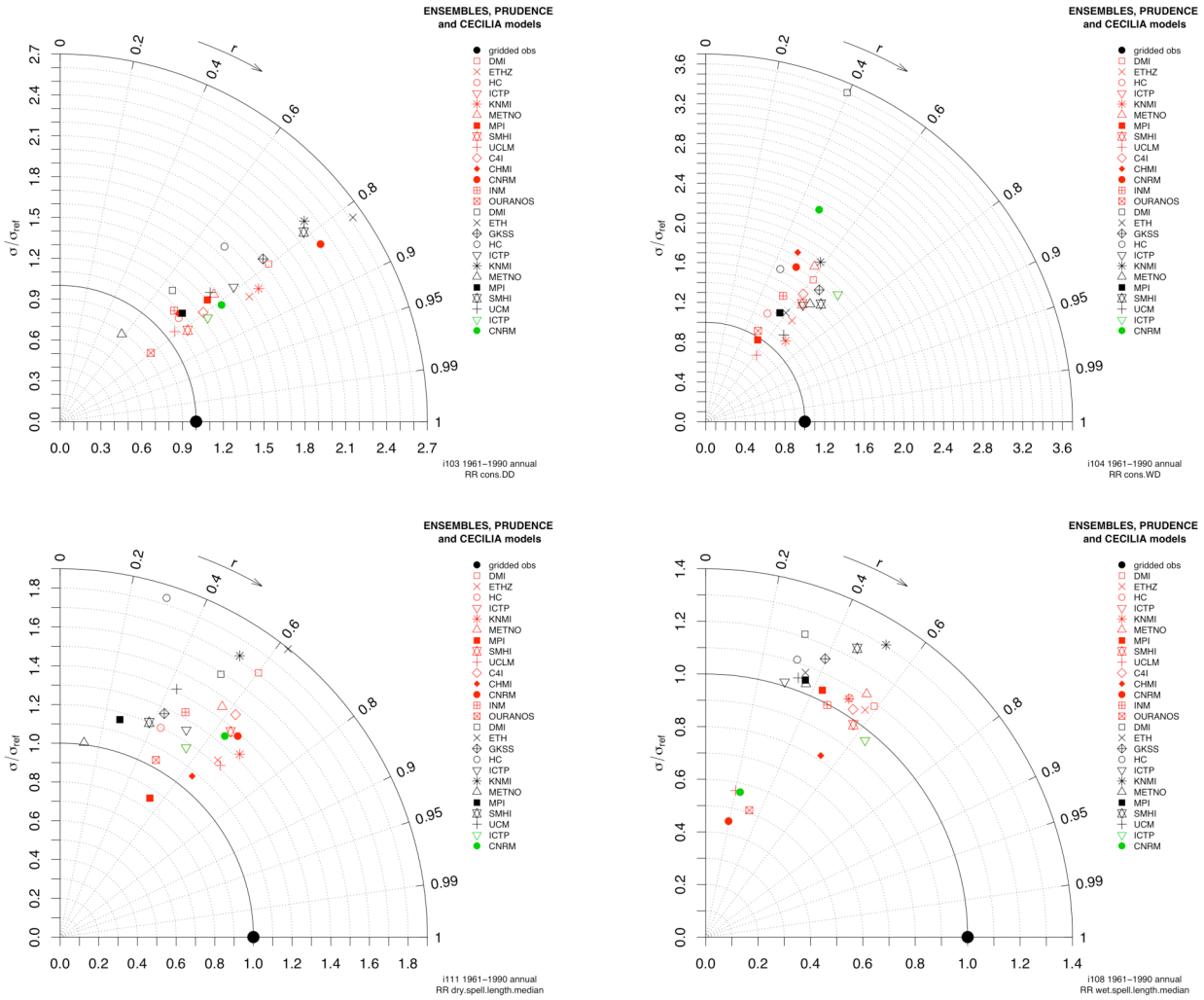
Figure 7. *As Figure 1, but for the derived precipitation indices displayed in Figure 6. (Top left) Max. number of consecutive dry days, (top right) max. number of consecutive wet days, (bottom left) median dry spell length, (bottom right) median wet spell length.*
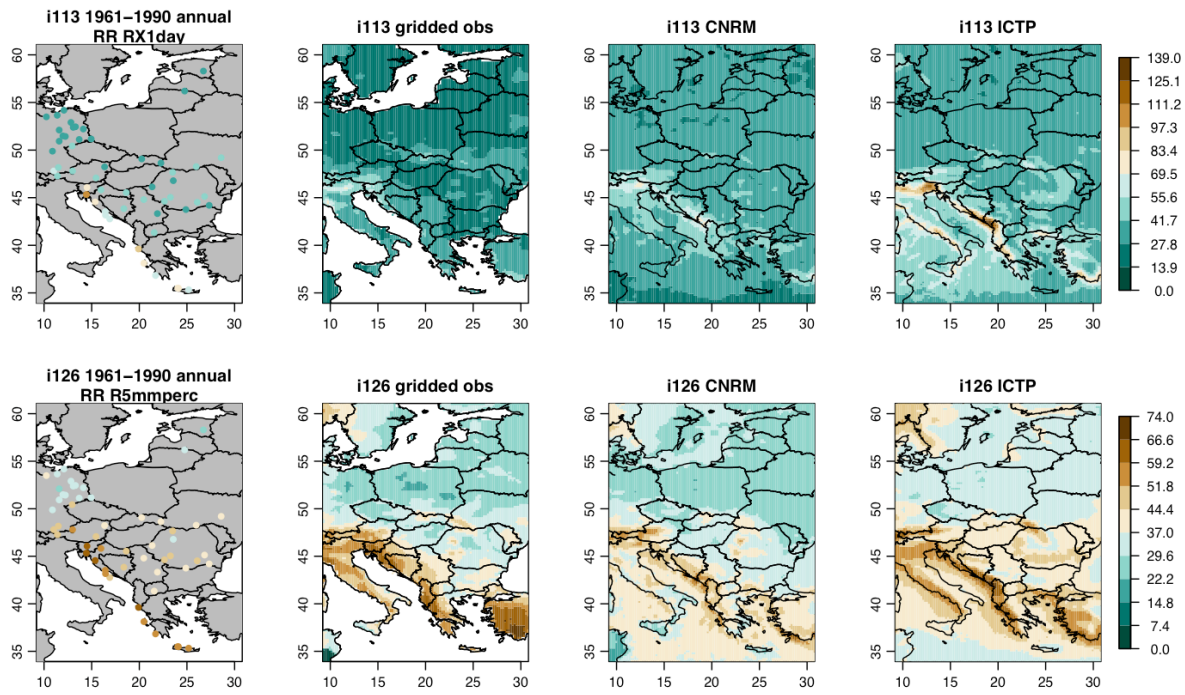
Figure 8. Comparison of other precipitation indices from the ECA&D station data, the ENSEMBLES gridded observations, and the CECILIA driving models. (Top row) greatest 1-day total rainfall [mm], (bottom row) percentage of wet days > 5mm [%].

D4.3.2 NMA: The link between regional-scale heavy precipitation in Romania and the large-scale circulation patterns using observational data

D4.3.2.1 Introduction
The nonhierarchical *K*-means clustering is used to classify the large-scale mean sea level pressure (MSLP) associated to heavy precipitation days in the intra-Carpathian region in Romania during all seasons for the period 1961-2006.

D4.3.2.2. Description of the data and methodology
Data
Daily precipitation totals from 30 Romanian stations (Fig.1) were used for the selection of the heavy precipitation days. The stations cover the intra-Carpathian area including the mountain stations bordering the area.
A heavy precipitation day was defined as that day when daily precipitation total exceeded a threshold depending on season.
The precipitation threshold was established by calculating the 95th and 97th percentiles, respectively, for each station and then selecting the average value of that percentile over the region.
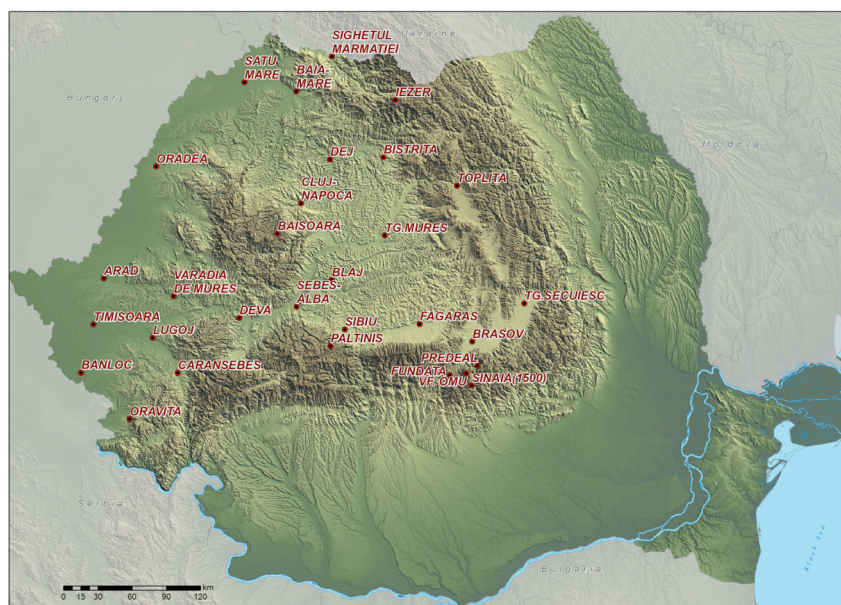

Figure 1. *The 30 Romanian (intra-Carpathian) stations used for the study.*

The period of the study covers the period 1961-2006 for all seasons (DJF, MAM, JJA, SON). As large scale data we used daily means of see level pressure (MSLP) and geopotential heights at 700 hPa from the NCEP/NCAR reanalysis data (http://www.cdc.noaa.gov/cdc/reanalysis/reanalysis.html) at 2.5ºx2.5º spatial resolution. The domain covers the Atlantic-European region (35–70ºN and 30ºW–50ºE).

Methodology
For station data:
- Selection of the days exceeding the thresholds (95th and 97th percentile) for daily precipitation amounts.

For the large scale data:
- For the MSLP and z700 fields the days exceeding the precipitation thresholds at stations were selected.
- Spatial standardizing the gridded data.

- Applying PCA on S-mode data matrix (the variables being the grid points and the days being the observations).
- The non-hierarchical K-means method was used to cluster the MSLP fields associated to the exceeding precipitation threshold days.
- To decide on the number of clusters and their centroids we considered the number of PCs exceeding 80% of the explained variance; the first 7 components were retained.
- To create the centroids (manual selection) of the clusters, days with high score values for a certain PC were selected (higher than +1 for the positive phase or lower than -1 for the negative phase, but imposing -1 and +1 for the rest of the PCs retained).
- Application of the K-means clustering with no iteration.
- The K-means procedure classifies all the days with similar distribution of the MSLP
- Regrouping the clusters into a smaller number of clusters to obtain the most representative circulation patterns associated to heavy precipitation in the intra-Carpathian region.

D4.3.2.3. Results

The patterns of the first 7 EOFs of MSLP associated to heavy precipitation exceeding 80% of the explained variance during winter (DJF) are represented in Figure 1. The corresponding EOF patterns for spring, summer and autumn (MAM, JJA and SOM) look very much alike to them.
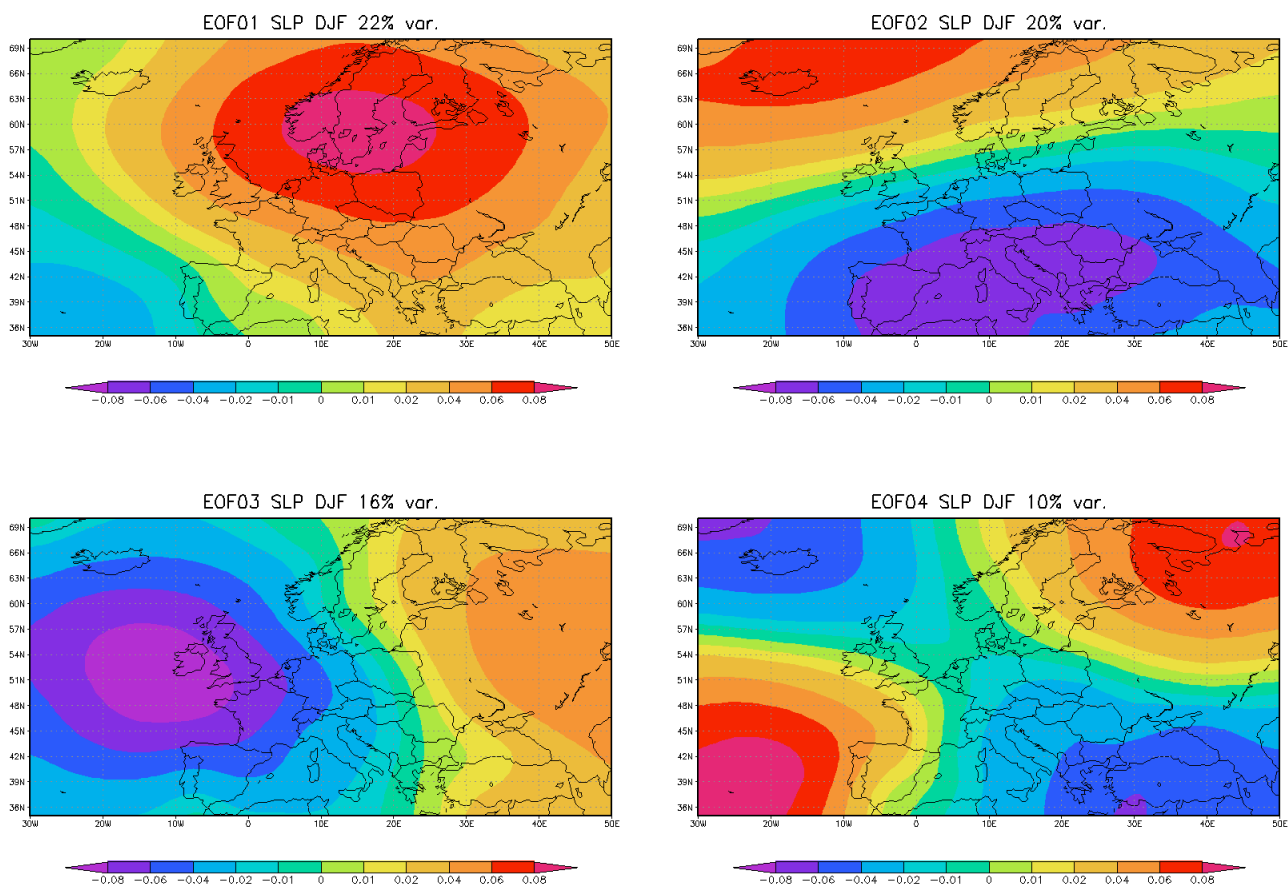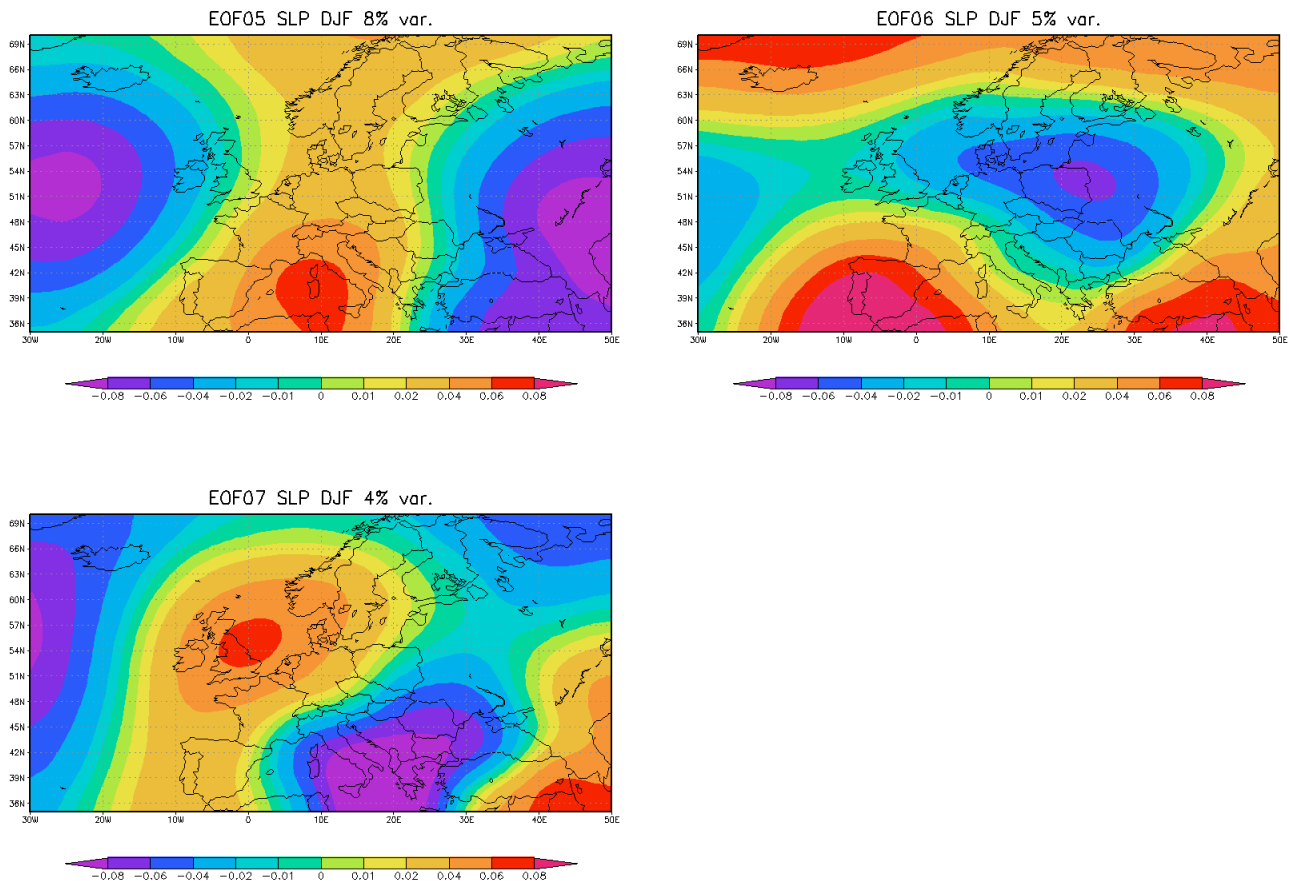
Figure 2. *The first seven EOFs for SLP during winter explaining more than 80% of the total variance.*

- After using the non-hierarchical K-means method to cluster the large-scale data associated to selected days exceeding precipitation thresholds and, after regrouping of clusters into a smaller number we obtained the most representative circulation patterns.
- The characteristic of the flow is relative to the intra-Carpathian region.
- In Figure 2 the most representative circulation patterns of the MSLP field and the corresponding Z700 field, associated to heavy precipitation in winter (DJF) are represented.
- The large-scale patterns associated to precipitation exceeding the selected thresholds are similar for all seasons.
- The distribution of the days exceeding the precipitation thresholds into clusters is uneven during the seasons and points out for the prevailing flows: zonal, high latitude zonal, SW and SE (European blocking).

Zonal circulation

Clus 1 SLP DJF

Clus 1 G700 DJF

990 994 998 1002 1004 1008 1012 1016 1020 1024 1030

270 276 280 284 288 292 296 300 304
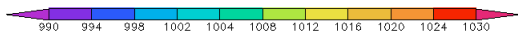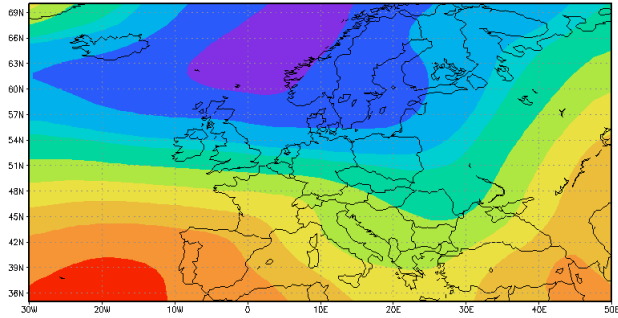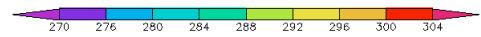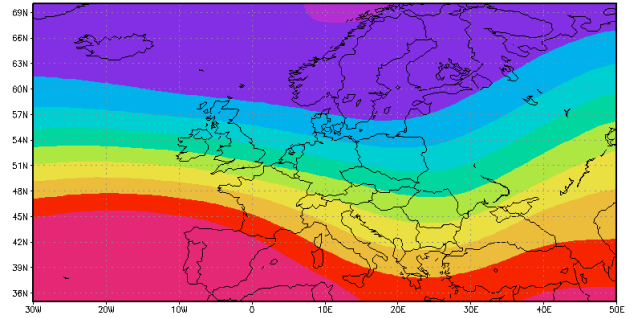
NW circulation

Clus 2 SLP DJF

Clus 2 G700 DJF

990 994 998 1002 1004 1008 1012 1016 1020 1024 1030

270 276 280 284 288 292 296 300 304
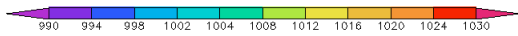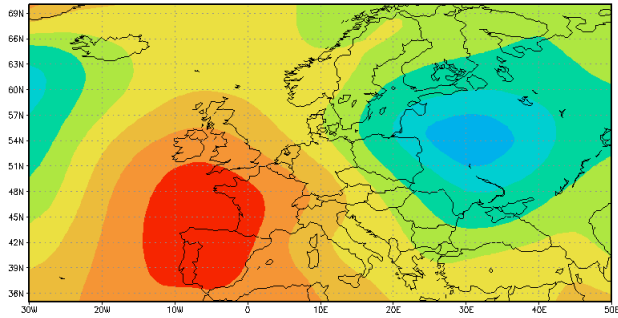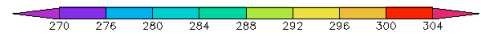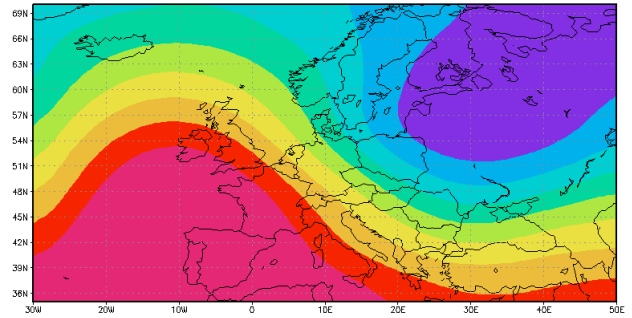
High latitude zonal circulation

Clus 3 SLP DJF

Clus 3 G700 DJF

990 994 998 1002 1004 1008 1012 1016 1020 1024 1030

270 276 280 284 288 292 296 300 304

SW circulation

Clus 4 SLP DJF

Clus 4 G700 DJF

E circulation

Clus 6 SLP DJF

Clus 6 G700 DJF
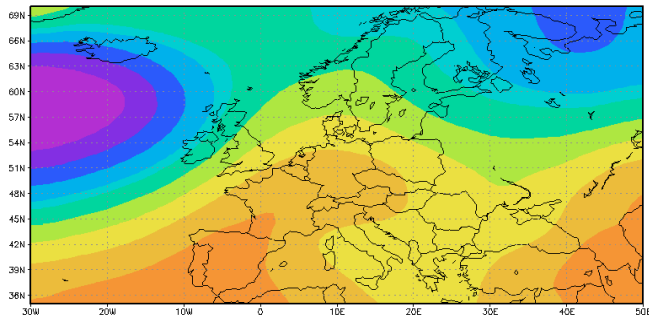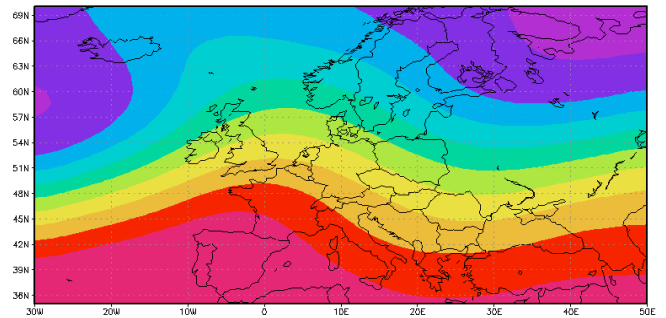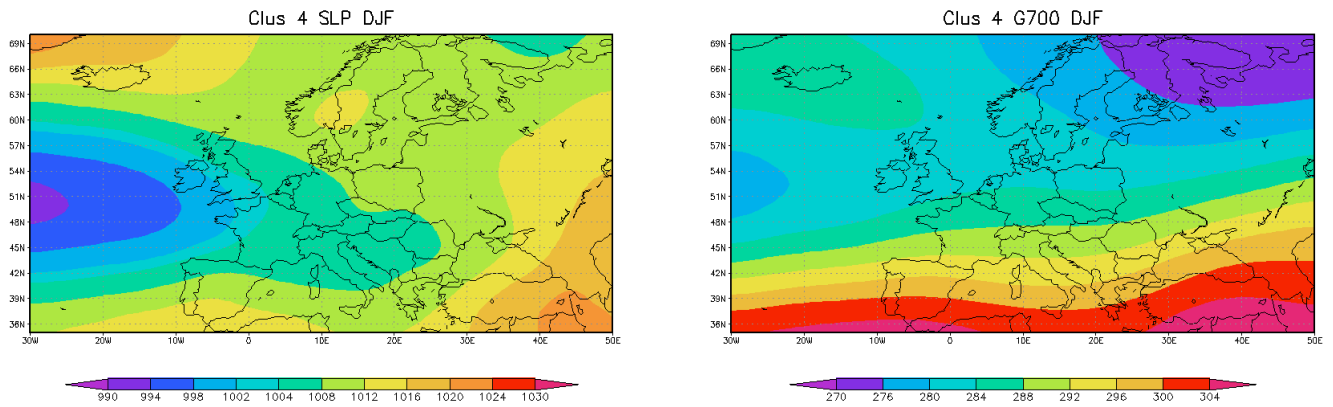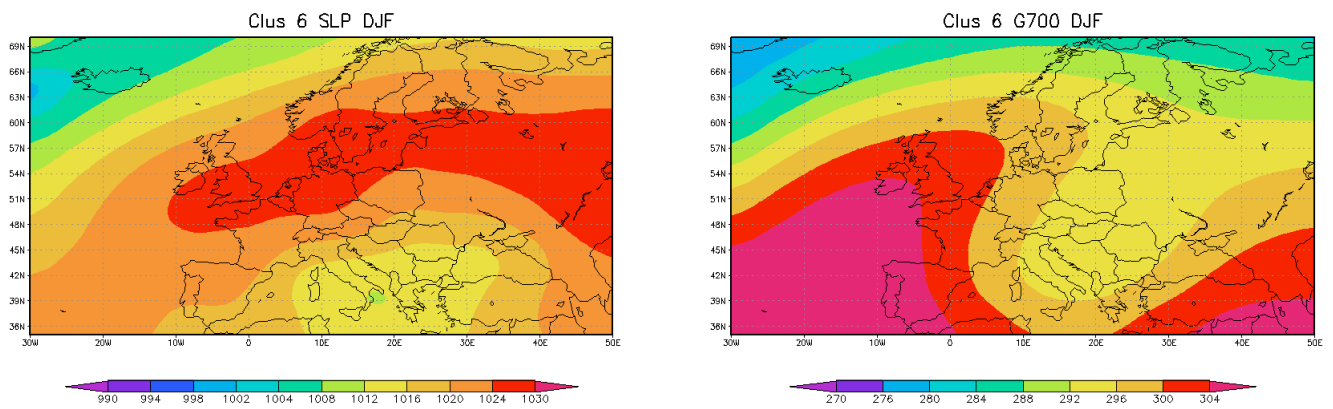
SE circulation (European blocking)

Clus 7 SLP DJF

Clus 7 G700 DJF
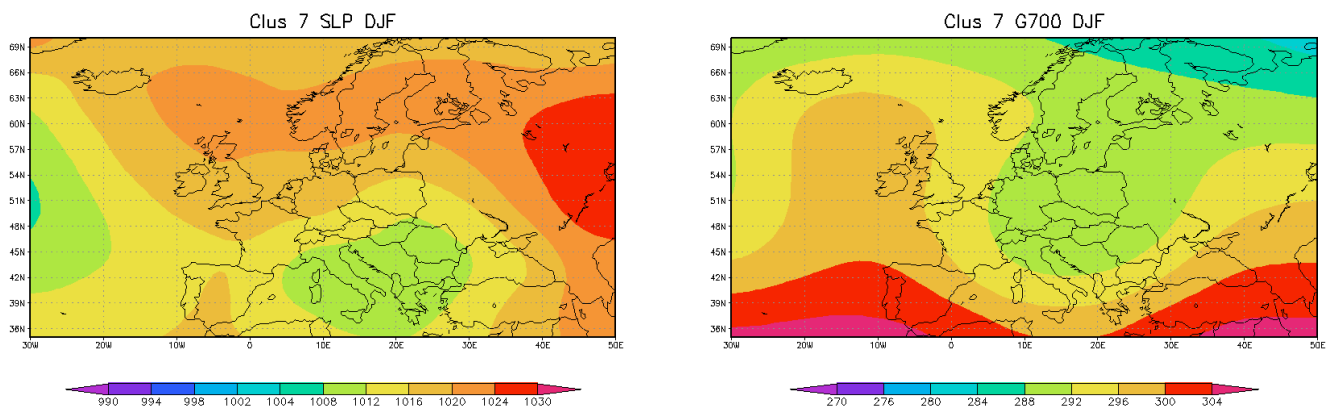
Figure 3. *The circulation patterns for SLP (left panels) and the corresponding z700 hPa (right panels) associated to heavy precipitation in the intra-Carpathian region of Romania.*

Table 1. *The distribution of the days exceeding various precipitation thresholds for different seasons.*

DJF: thr: 15 mm; 535 days

| Cluster 1	Cluster 2	Cluster 3	Cluster 4	Cluster 5	Cluster 6
Zonal	NW	High lat zonal	SW	E	SE (European blocking)
82	50	104	132	65	102

MAM1: thr: 15 mm ; 994 days

Cluster 1	Cluster 2	Cluster 3	Cluster 4	Cluster 5	Cluster 6
Zonal	NW	High lat zonal	SW	E	SE (European blocking)
165	11	206	224	130	158

MAM2: thr: 20 mm ; 619 days

Cluster 1	Cluster 2	Cluster 3	Cluster 4	Cluster 5	Cluster 6
Zonal	NW	High lat zonal	SW	E	SE (European blocking)
95	49	137	140	86	112

JJA1: thr: 30 mm ; 762 days

Cluster 1	Cluster 2	Cluster 3	Cluster 4	Cluster 5	Cluster 6
Zonal	NW	High lat zonal	SW	E	SE (European blocking)
128	76	156	177	102	123

JJA2: thr: 35 mm ; 529 days

Cluster 1	Cluster 2	Cluster 3	Cluster 4	Cluster 5	Cluster 6
Zonal	NW	High lat zonal	SW	E	SE (European blocking)
77	49	99	127	71	106

JJA3: thr: 40 mm ; 370 days

Cluster 1	Cluster 2	Cluster 3	Cluster 4	Cluster 5	Cluster 6
Zonal	NW	High lat zonal	SW	E	SE (European blocking)
67	39	88	63	49	64

SON1: thr: 15 mm ; 789 days

Cluster 1	Cluster 2	Cluster 3	Cluster 4	Cluster 5	Cluster 6
Zonal	NW	High lat zonal	SW	E	SE (European blocking)
127	86	168	180	103	125

SON2: thr: 20 mm ; 524 days

Cluster 1	Cluster 2	Cluster 3	Cluster 4	Cluster 5	Cluster 6
Zonal	NW	High lat zonal	SW	E	SE (European blocking)
102	59	116	85	68	94

D4.3.3 AUTH

Large-scale circulation patterns, such as the ones connected to the North Atlantic Oscillation (NAO) are known to control westerly flow of air into the European continent, thus affecting local weather and climate. Our aim is to investigate their effects in detail over Europe, and specifically their relation to temperature and precipitation changes using high-resolution data.

To achieve this, we use data from simulations performed with General Circulation Models that were used as driving models for the Regional Climate Models (RCMs) in the framework of the CECILIA project. Here we use data from 3 simulations performed with the GCM ARPEGE.4.5 for the periods 1950-2000 (control), 2001-2050 and 2051-2100 that were made available to us.

NAO related effects:
We have defined the NAO Index for the 3 subperiods mentioned above using daily sea level pressure (slp) data from the simulations. We chose the grid-points closest to Ponta Delgada, Azores and Stykkisholmur/Reykjavik, and the index of the NAO was calculated from the daily means based on the difference of normalized sea level pressure (SLP) between the two grid points. The main focus is in northern winter (December through February), when the effects are more pronounced, so the winter mean index was calculated. Years of high (or low) NAO Index were then defined as belonging to the upper (or lower) quartile (25% or 75%) of the data.
From the daily mean data sets we defined as days of high (or low) NAO index the days pertaining to the high or low Index winters. The daily mean Index for each day had to be above or below zero so that the day could be categorized as a high Index day (or low Index day respectively).

We have used temperature (mean, maximum and minimum) and precipitation data as daily means. For each of the three subperiods we calculated the long-term daily average, which was subsequently subtracted from the data so as to have departures from the mean. As a next step, we calculated composites for the winters with positive and negative Index using only the days pertaining in each case.
Figure 1 shows the results for the daily mean temperature. The top row presents the composites from the daily means pertaining to days with high (positive) Index, while the bottom row for the days with low (negative) Index. The significance of the changes was tested against the long-term winter average for all days. The lack of coloring denotes area where the changes were not significant above the 95%level).
Results for precipitation are presented in Figure 2.
The main results were similar to the observed NAO effects over Europe, i.e. warm and wet over North-Eastern Europe and dry over the Mediterranean when NAO is in the positive phase (positive NAO Index, top rows in both cases). The magnitude of these effects appears to be larges during the negative phase, the changes being the largest over Scandinavia and the Baltic Sea.
Comparison of the three sub periods reveals that these changes become stronger as we move into the 21st century, with the last 50-year period showing the strongest effects.
The above results are seen not only in average daily mean temperature, but in daily maximum and minimum temperatures as well. It should be noted that the effect is large in daily minimum temperatures over greater areas. In the case of precipitation, Mediterranean (and its northern surrounding area) is found to become drier for positive changes of NAO Index, while central and northern Europe experience more wet weather.
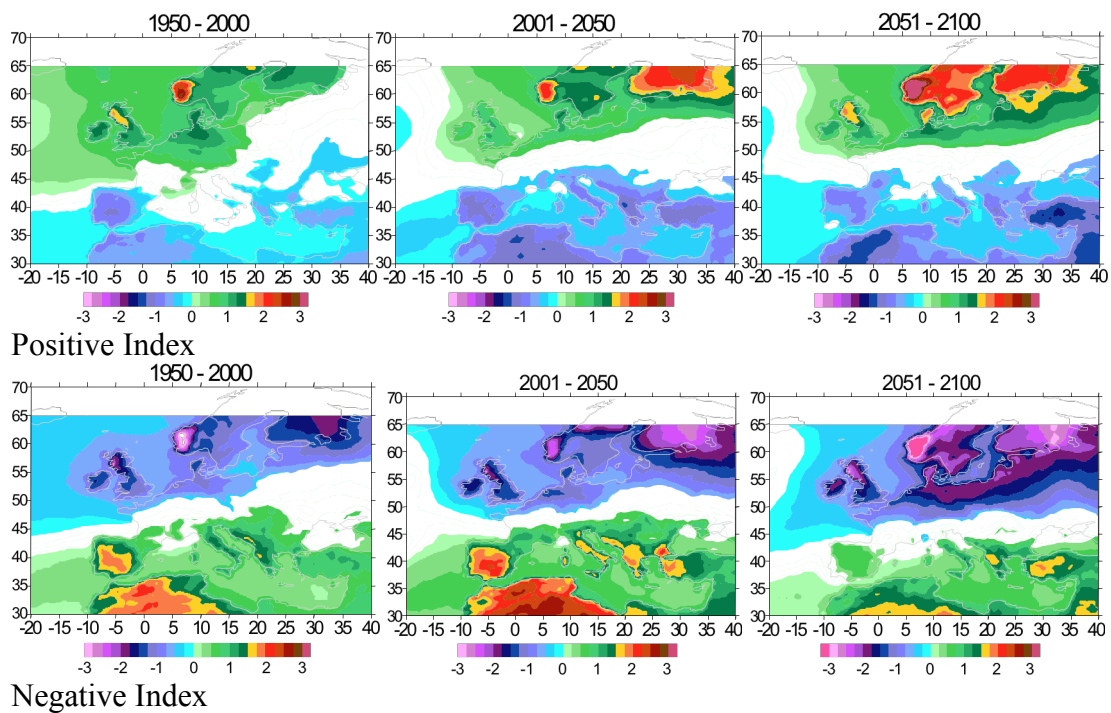
Figure 1. *Winter (DJF) composites of daily mean temperature during days related to positive changes of the normalized NAO Index (top row) and negative changes (bottom row). The three sub periods, 1950-2000, 2001-2050 and 2051-2100 are shown from left to right. Only areas with significant effects are plotted (>95% as deduced with Student's t-test).*
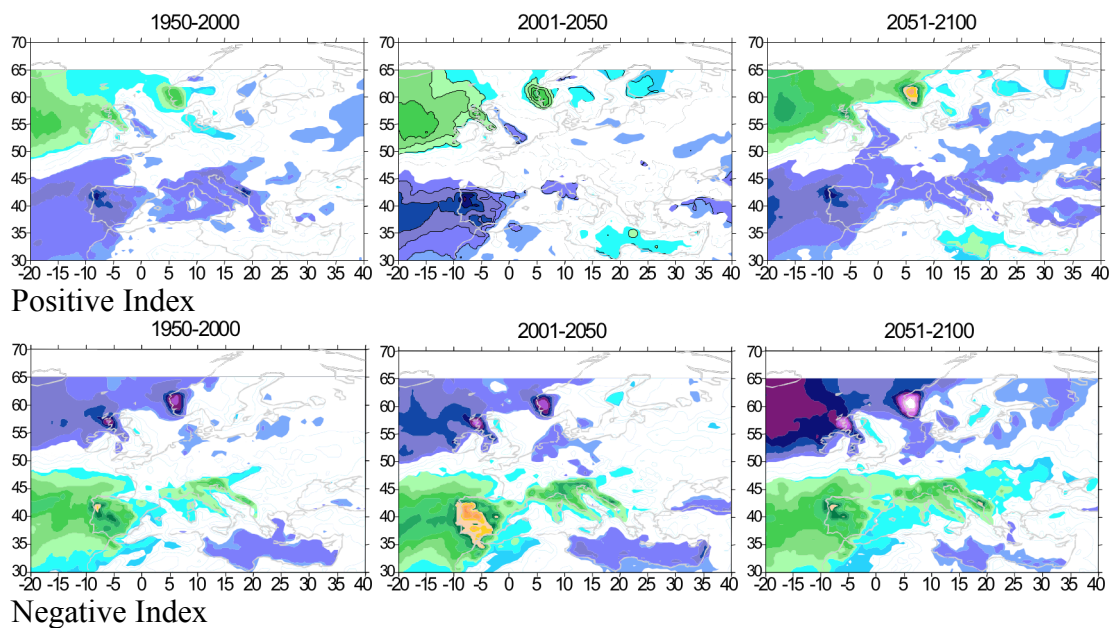

Figure 2. *Same as Figure 1 but for daily mean precipitation (top row positive Index, bottom row negative Index). Blue color scale denotes drier and colder areas.*

D4.3.4 References

Haylock, M. R., Hofstra, N., Klein Tank, A. M. G., Klok, E. J., Jones, P. D., and New, M. (2008). A European daily high-resolution gridded dataset of surface temperature and precipitation for 1950–2006. Journal of Geophysical Research, **113**(D20119):doi:10.1029/2008JD010201.

Klein Tank, A., et al. (2002). Daily dataset of 20th-century surface air temperature and precipitation series for the European Climate Assessment. *Int. Journal of Climatology*, **22**(12):1441–1453.

Taylor K. E. (2001). Summarizing multiple aspects of model performance in a single diagram. *Journal of Geophysical Research*, **106**(D7):7183–7192.